Copper Mediated Hydrothermal Synthesis of Ultra Long Pentagonally Twinned Palladium Nanowires

Jennifer Hanson

A thesis

submitted in partial fulfillment of the

requirements for the degree of

Master of Science

University of Washington

2014

Committee:

Peter Pauzauskie

Dwayne Arola

Kannan Krishnan

Program Authorized to Offer Degree:

Material Science Engineering

University of Washington

Abstract

Copper Mediated Hydrothermal Synthesis
of
Ultra Long Pentagonally Twinned Palladium Nanowires

Jennifer Hanson

Chair of the Supervisory Committee:

Professor Peter Pauzauskie

Materials Science Engineering

Palladium nanowires (PdNWs) have attracted considerable attention due to applications in hydrogen sensing and heterogeneous catalysis. Several methods have been reported for the synthesis of PdNWs including using chemical vapor transport, electrodeposition in porous membranes, and colloidal self-assembly; however, it has been challenging to produce large quantities. Hydrothermal methods have been reported recently for the production of high yields of palladium nanowires using palladium (II) chloride as a metal precursor, deionized water as the solvent, and polyvinylpyrrolidone for the NW capping agent. Reported prior methods have not been reproducible. With the introduction of trace amounts of Copper (II) ions synthesis is possible and aspect ratios of >450 have been obtained. It is likely that the deionized water used in the synthesis contained trace amounts of copper from metal pipes, thus leading to the synthesis of PdNWs. Copper ions have been shown to act as effective oxygen scavengers during the aqueous synthesis and we postulate that oxidative etching of multiply pentagonally twinned palladium seeds must be avoided in order to achieve high yields of palladium nanowires.

Table of Contents:

I. Introduction:

Palladium nanocrystals have attracted a considerable amount of recent experimental attention due to applications in hydrogen sensing[1][2], crystal-facet-dependent singlet-oxygen generation[3], and heterogeneous catalysis[4]. Several methods have been reported for the synthesis of Palladium nanowires and whiskers using chemical vapor transport[5][6], electrodeposition[7][8] in porous membranes[9][10], electron beam lithography[11], colloidal self assembly[6][12][13], and dielectrophoresis[14]. In contrast with synthesis of gold and silver nanowires *via* soft templating in solvothermal reactions, to date it has been challenging to produce large quantities of palladium nanowires due to fundamental differences in electrochemical redox potentials between noble metals with face-centered cubic (FCC) crystal structure. In the case of palladium, the redox potential is low enough that kinetics are substantially slower than in the case of gold and silver nanowires, making it difficult to achieve nanowire morphologies when conducting synthesis reactions near standard temperature and pressure. Furthermore, in solvothermal reactions the final morphology of nanocrystals is determined by a combination of rate-limited kinetic control of crystal facet growth in tandem with an overarching thermodynamic constraint of minimizing the particle's total surface energy. It is well known that for face-centered cubic (FCC) metals their relative surface energies usually increase in the order $a_{\{111\}} < a_{\{100\}} < a_{\{110\}}$ corresponding to {111}, {100}, and {110} Miller indices, respectively. In the limit of thermodynamic control the final particle morphology is determined by a particular morphology that minimizes the total surface energy of the nanocrystal.

Hydrothermal methods have been reported recently for the production of high yields of palladium nanowires using palladium (II) chloride as a metal precursor, deionized water as the solvent, and polyvinylpyrrolidone for the nanowire capping agent[15]. The reported prior

methods[15] have not been reproducible in the present authors' hands. In this manuscript it is shown that copper (II) ions are a critical component for palladium nanowire synthesis. The critical importance of copper ions in the synthesis of Palladium nanowires has not been reported to the best of the authors' knowledge.

Copper ions have been shown to act as effective oxygen scavengers during the aqueous synthesis of silver nanowires[16]. We postulate that oxidative etching of multiply pentagonally twinned palladium seeds must be avoided in order to achieve high yields of palladium nanowires. In prior reports of hydrothermal palladium nanowire synthesis[15] it is likely that the dionized water used in the synthesis contained trace amounts of copper from metal pipes, thus leading to the synthesis of Palladium nanowires.

II. Literature Review

II.1 FCC Metallic Nanoparticle Growth and Synthesis

The first stage of nanocrystal synthesis is nucleation – a process in which miniscule clusters of a few atoms or ions called nuclei are formed. Thus far attempts to probe, comprehend, and control this process have had limited success[17]. A lack of experimental tools capable of identifying and monitoring the nuclei has been a crucial challenge, making direct observation of formation in real space remarkably difficult[18][19]. To compensate scientists have relied on theoretical approaches to simulate and account for nucleation [20]. Model systems with larger building blocks of colloidal spheres have been employed as well [21]. While these systems can be studied optically, there are limitations with respect to differences in surface properties, interaction potential, and solvation. Finally nucleation has been studied on flat surfaces using scanning probe microscopy [22][23][24].

Typical metallic nanocrystal syntheses start with the decomposition or reduction of a precursor to generate zero-valent atoms, which are the building blocks of the crystal. The nucleation process is therefore dependent on the explicit route to these zero-valent atoms. The precursor decomposition route follows from the mechanism by developed LaMer in the 1950s for sulfur colloids [25]. Briefly for metallic nanoparticles, the precursor decomposes with heat or sonication, providing a steady increase in the metal atom concentration. Upon supersaturation, atoms aggregate into small clusters via homogeneous nucleation. These nuclei grow through atomic addition into nanocrystals, removing metal atoms from solution and eventually decreasing the metal atom concentration as the precursor is used. Nucleation events stop as the metal atom concentration drops below minimum supersaturation.

The precursor reduction route entails reduction of a higher oxidation state precursor to zero-valent atomic compounds. The precursor can either be reduced to zero-valent atoms that aggregate/grow or nuclei can be formed prior to reduction from unreduced species [18][19]. The later is only favorable under certain experimental conditions (mild reducing agent and/or high precursor concentration). Furthermore, the nuclei might not be fully reduced to a zero-valent state as the surface can be terminated by positively charged metal ions that are solvated or coordinated to ligands. This is similar to and related to the capping effect of ionic species (Cl-, Br-, citrate) and polymers for the nanocrystal growth [19].

Beyond a critical size, the cluster confined to a specific well-defined structure, known as a seed, as structural fluctuations become too energetically costly. Seeds can be seen as an intermediate in the evolution of nuclei to nanocrystal and may be single-crystal, singly twinned, or multiply twinned in nature as seen in fig. 1. Reactions can contain multiple seed types and one primary aim of directed synthetic effort in obtaining nanocrystalline shapes to willfully obtain a

solution of one seed type excluding or greatly limiting others. Essentially seed structure is

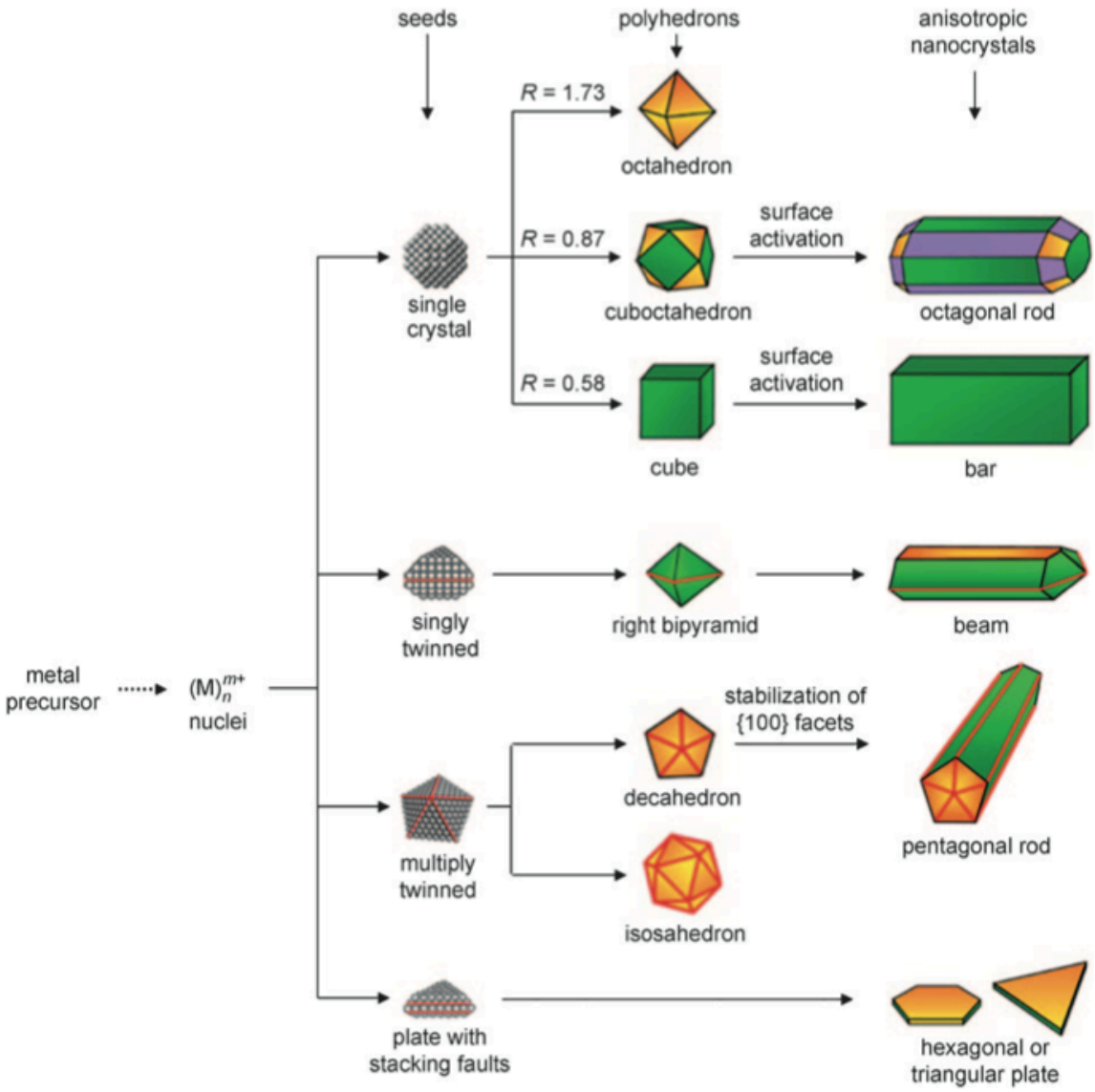

Figure 1 | Nanocrystal Seed Geometries
Seeds can have single-crystal, singly twinned, or multiply twinned structures. Stacking faults produce plate-like seeds. Colors represents twin planes (red lines) and differing crystal facets green {100}, orange {111}, and purple {110}. R is defined as the ratio between the growth rates along the <100> and <111> directions[18].

determined by an interplay of threnodynamic and kinetic controls of atomic metal adsorption onto the growing cluster along with external/other processes such as oxidative etching.

The thermodynamic control produces the greatest proportion of most stable product. Stability in the simplest sense, for single-crystal seeds, can be conferred through the minimization of total interfacial free energy of the system per given volume via Wulff's theorem. Mathematically this is the partial derivative of free energy with respect to surface area while holding temperature, pressure, and number of atoms constant. As a model, forming seeds have missing bonds at the surface that break the crystal symmetry and cause the surface atoms to be attracted toward the interior. Per force balance, a restoring force is needed to push back these atoms toward initial positions. Thus for an idealized surface, interfacial energy is given by the product of the number of broken bonds, the bond strength, and density of atoms on the surface. Using this model for an FCC structure, energetic sequences of low-index crystallographic facets can be compared to give free energies: $g\{111\} < g\{100\} < g\{110\}$, indicating single-crystal seeds should primarily have octahedral and tetrahedral shapes to maximize {111} surfaces [26]. These shapes have larger surface area as compared to a cube of the same volume such that truncated structures minimizing total interfacial free energy and surface area are generally obtained[26]. Beyond single-crystal seeds, singly and multiply twinned seeds are possible. Singly twinned seeds are enclosed by a mixture of {111} and {100} facets to minimize total interfacial free energy[27][28] . Multiply twinned seeds have a more complex nature as the twin defects induce significant size-dependent strain energies. A decahedral seeds that has five-fold twinning can be viewed as a set of five single-crystal tetrahedral units sharing a common edge with each tetrahedron containing two sides in contact with a neighbor via {111} twin planes. The theoretical angle between {111} planes of a tetrahedron does not fit a 360-degree closure and leaves a gap of 7.358 degrees (fig. 2) that stretches the bond lengths between adjacent atoms.

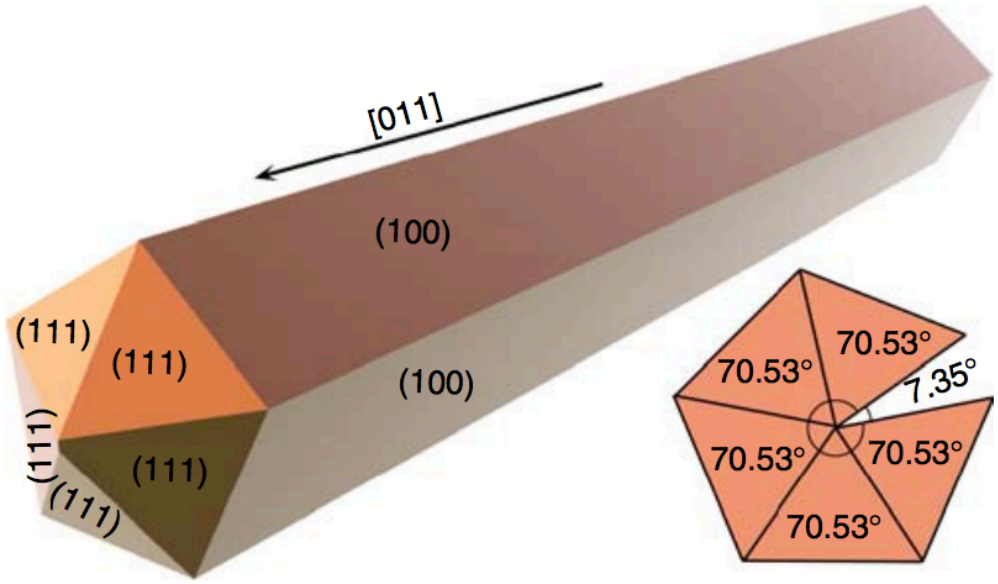

Figure 2 | Pentagonally Twinned Nanowire Structure

The symmetry of pentagonal twinning leaves a sizable gap of 7.35 degrees inducing strain energy [9].

This causes internal lattice strain and disordered, high-energy regions at the boundaries [29][30]. Thus multiply twinned seeds are favored at relatively small sizes and there is a critical relationship between size-dependence and seed type [31].

The kinetic control relates to additional strain energy caused by defects such as twinning or stacking faults and the interplay between this strain energy and overall surface energy [28][32]. Other processes such as oxidative etching occur due to additional reagents in the solution environment and competing reactions. Oxidative etching is a process in which zero-valent metal atoms are oxidized back into ions. As most syntheses are conducted in air, oxygen dissolved in the aqueous solution through the ambient environment is present throughout the synthesis. This oxygen absorbs onto surfaces of growing nanoparticles such that it can oxidize the zero-valent metal into higher oxidation ionic states, allowing for easy removal of the atoms if a ligand for the metal ion is present in the solution. This is a powerful etchant for nuclei and seeds. As defect zones are higher in energy compared to single-crystal regions, they are more susceptible to oxidative etching. Thus oxidative etching is selective in the removal of twinned crystals. This phenomenon has been shown for both silver and palladium nanoparticles[33][16]. In a polyol synthesis of silver nanocrystals, all multiply twinned seeds can be selectively removed from the solution via the addition of trace amounts of chloride leaving a distribution of single-crystal nanoparticles[33]. Trace amounts of counter ions of metal precursors or ionic impurities can have significant impacts on oxidative etching and seed population as well. For common precursors such as Na2PdCl4 used in Pd nanocrystal synthesis, the chloride ion contributes significantly to oxidative etching and leaves only single-crystal cubooctahedra seeds [34].

II.2 Applications of Palladium Nanoparticles

II.2.1 Palladium as a Catalyst

Palladium has been used prominently in organic chemistry as a catalyst for hydrogenation and dehydrogenation reactions as well as cracking. The catalyst is based on zero-valent metallic Palladium and its complexation derivatives for the formation carbon-carbon (C-C) bonds also known as cross-coupling. Beyond pure organic synthesis for production of chemical production, Palladium is used in catalytic converters. It can convert up to 90% of the harmful gases such as carbon monoxide and nitrogen monoxide from auto exhaust into less harmful substances such as carbon dioxide and nitrogen gas[35].

The Palladium catalyst allows for a host of elementary reactions to occur via the C-C bond formation under mild environments. As such, it has revolutionized the field of organic chemistry allowing for a simplistic route to small molecule synthesis. Understanding and developing this catalyst has even garnered the 2010 Nobel prize in chemistry for Akira Suzuki Richard F. Heck and Ei-ichi Negishi[36]. By changing the reagents several prominent reactions mechanisms occur. Briefly, the Mizoroki-Heck Reaction reacts unsaturated halide and alkene under basic conditions with Palladium catalyst to form a substituted alkene. It allows for the substitution reaction on planar sp2-hybridized carbon centers and was the first C-C bond forming reaction to use a metallic-ionic Pd(0)/Pd(II) catalytic cycle similar to the later proposed Suzuki reaction[37]. The Suzuki reaction reacts organoboron species (R1-BY2) and a halide (R2-X) with a similar Pd(0)/Pd(II) catalytic cycle as can be seen in figure 3[38]. The Songoshira synthesis utilizes terminal alkyne and an aryl or vinyl halide for the cross coupling[39]. The Hiyama uses organosilanes and organic halides as reagents and preserves both chemo- and regioselectivity[40].

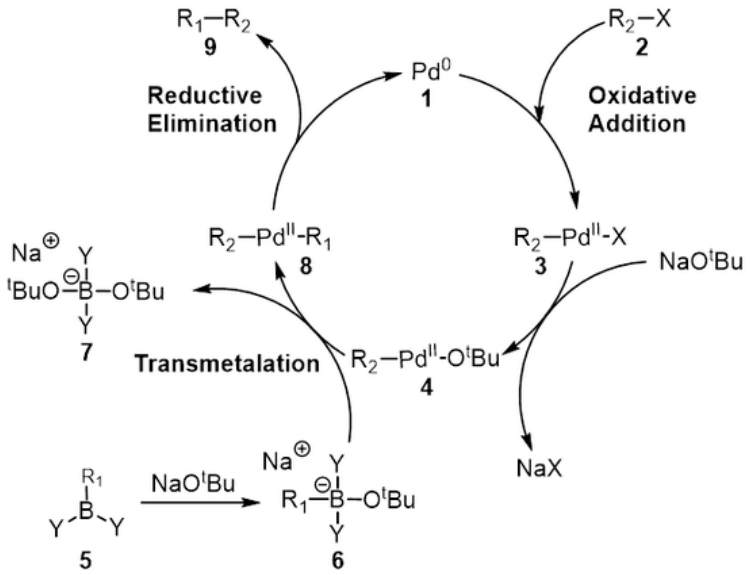

Figure 3 | Suzuki Mechanism

Oxidative addition of Palladium metal (1) and halide (2) forms organopalladium compound(3) which reacts with base to give intermediate(4). Transmetalation of (4) with complex (6) forms the organopalladium species (8), which undergoes RE to produce desired product (9) and original Palladium catalyst.[41][37][38]

Suzuki Reaction Scheme[38]:

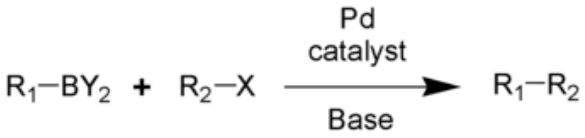

Mizoroki-Heck Reaction Scheme[41]:

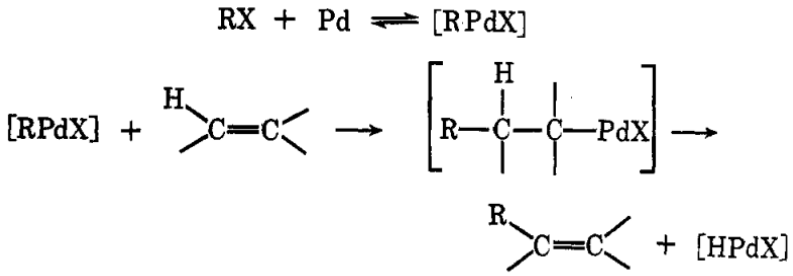

Hiyama Coupling Scheme[40]:

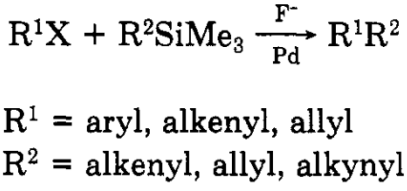

Figure 4 | Reaction Schema Using Palladium as a Catalyst

II.3 Palladium as a Hydrogen Storage Medium

Palladium can adsorb substantial quantities (up to 900 times its own volume of H2 at room temperature and atmospheric pressure) of hydrogen to form palladium hydride, an alloy of palladium with metallic hydrogen[42]. The adsorption is reversible and thus has been studied for hydrogen storage[43] and sensing[44] applications.

Two crystalline phases, α and α‘, form with varying hydrogen adsorption. Depending on atomic ratio of palladium to hydrogen (PdH_x), pure α phase ($x < 0.017$), pure α‘ phase ($x > 0.58$) and α –α‘mixtures (intermediate x values) are possible as can be seen in fig. 5. Both phases contain palladium atoms in the native metallic face centered cubic (fcc) lattice structure. The lattice expands from 3.889 Å to 3.895 Å with low concentrations of hydrogen adsorption up to $PdH_{0.02}$. The second phase then appears with a noticeable expansion of the lattice constant to 4.025 Å. Both phases coexist until a composition of $PdH_{0.58}$ when the only the secondα‘ phase remains.[42]

Surface adsorption kinetics were examined through scanning tunneling microscopy (STM) on Pd(111) surface. Aggregates of at least three vacancies on the crystal surface (fig 6) are required to promote dissociation of the diatomic hydrogen molecule [45]. This contradicts the classical Langmuir picture of second order adsorption kinetics in which pairs of sites are required.[46] The reason for such a behavior and the particular structure of trimers has been analyzed. Experiments find that at least three empty sites are needed. Through density functional theory, we find that H_2 dissociation is favored on ensembles of sites that involve a Palladium atom with no direct interaction with adsorbed hydrogen. Such active sites are formed by aggregation of at least 3 H-free sites revealing the complex structure of the ‘‘active sites.’’[46]

Neutron diffraction studies have shown that hydrogen atoms randomly occupy the octahedral interstices in the metal lattice (in an fcc lattice there is one octahedral hole per metal

atom). The limit of absorption at normal pressures is $PdH_{0.7}$, indicating that approximately 70% of the octahedral holes are occupied. The absorption of hydrogen is reversible, and hydrogen rapidly diffuses through the metal lattice. Metallic conductivity reduces as hydrogen is absorbed, until at around $PdH_{0.5}$ the solid becomes a semiconductor.[47]

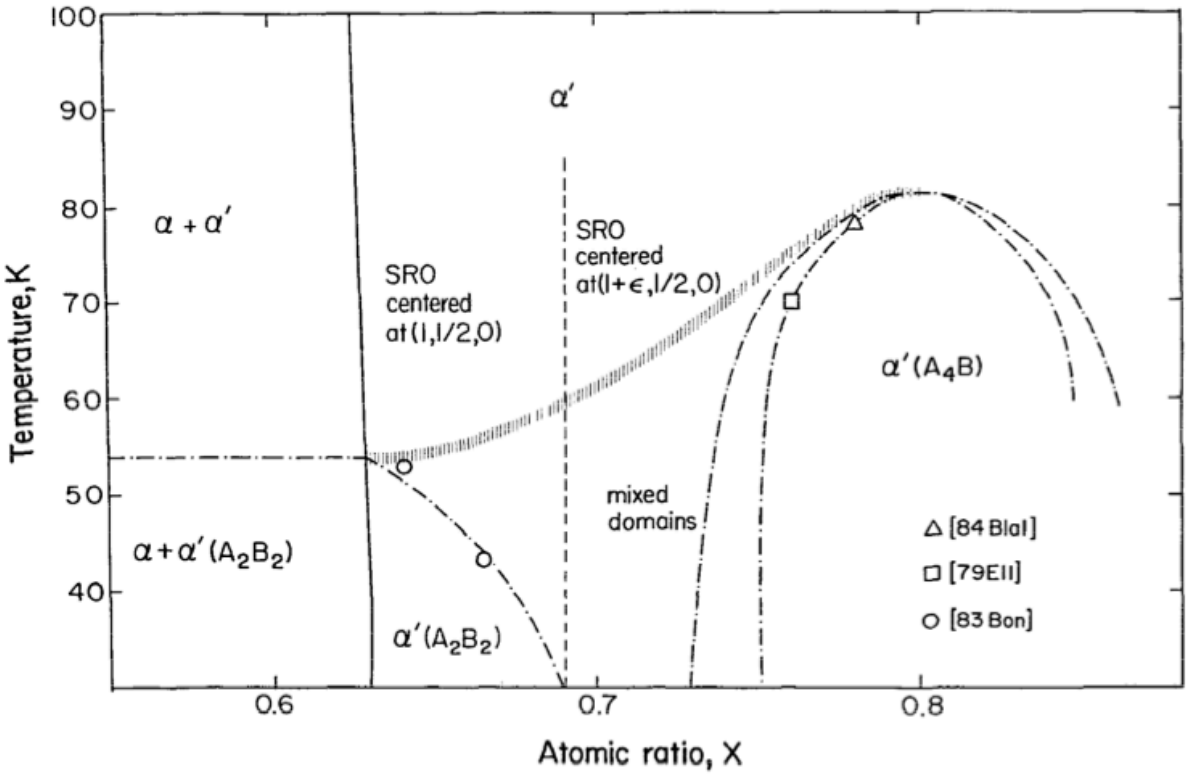

Figure 5 | Palladium Hydride T-X Diagram
T-X diagram for high-concentration, low-temperature region. Phase boundaries are shown via solid lines; onset of ordering via dot-dashed lines [42].

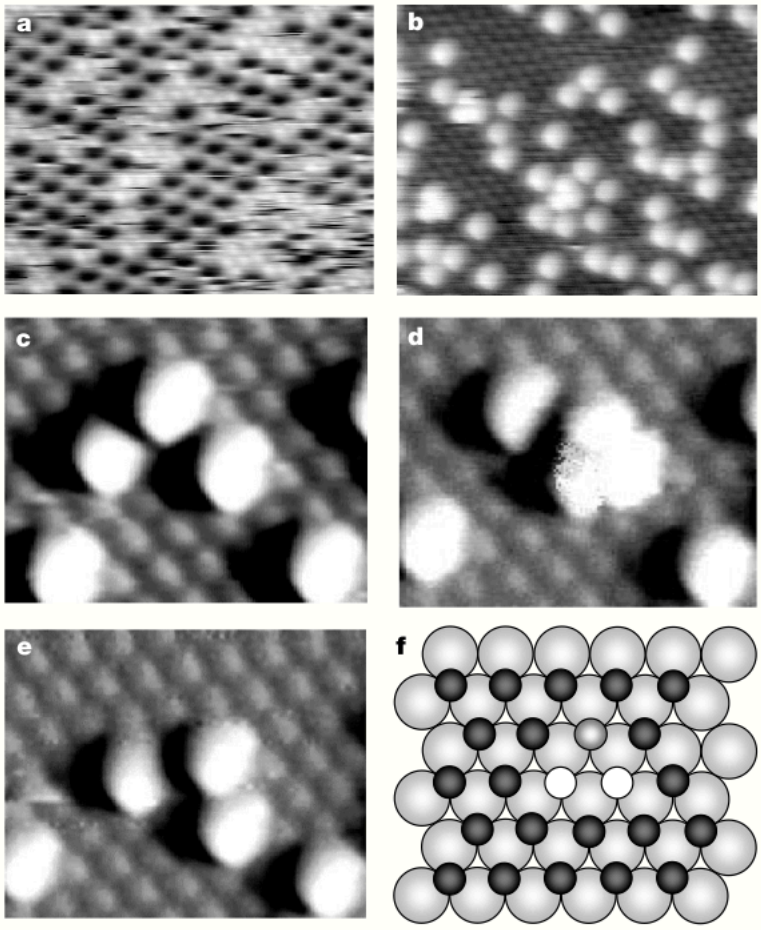

Figure 6 | STM images of hydrogen atoms on Pd(111)
STM images show absorption of hydrogen to requires aggregates of at least three vacancies on the surface of the crystal to promote the dissociation of the hydrogen molecule. The H-atom (light-shaded) can rapidly exchange with the vacancies (white circles) by hopping over bridge sites that offer smallest barrier to diffusion [45].

III. Materials and Methods

III.1 Synthesis of Palladium Nanoparticles.

In a typical synthesis, 17.7mg (0.1 mmol) of palladium dichloride (PdCl2, Aldrich, lot#MKBJ3841V), 300 mg (2 mmol) of sodium iodide (NaI, Sigma-Aldrich, lot#BCBD5784V), and 800mg (MW) of polyvinylpyrrolidone (PVP, MW 55000, Sigma-Aldrich, lot#MKBC3440V) are added to a round bottom flask. 11mL of 18.6 MΩ·cm water (Millipore) is added to the flask and the mixture of reagents is sonicated until the PVP dissolves completely. For experiments with copper (II), 1mL of copper acetate solution (Cu(OAc)2*H2O Sigma-Aldrich, lot#MKBF3566V) is added dropwise to the solution after PVP is dissolved.

The solution is stirred at 50°C for 10 hours and then sealed within a 25 mL Teflon-lined autoclave (Parr, model#4749). The sealed autoclave is then heated in an oven or silicon oil bath in a temperature range between 170°C and 220°C for times ranging between 2 hrs and 48 hrs, and then removed from the oven and allowed to cool to room temperature. The recovered solution is diluted with isopropyl alcohol, and then repeatedly rinsed and centrifuged at 5000 rpm. Samples are finally rinsed and suspended in ethanol or water before subsequent characterization. Vials containing high-aspect-ratio nanowire suspensions are observed to have a dynamic opalescent texture when inverted.

III..2 Synthesis of Palladium Nanoparticles with Iron Control.

Experiments with ferrous sulfate heptahydrate (JT Baker, lot#J20623) were carried out in as described above. Briefly 1 mL of 8mM ferrous solution replaced the copper(II) solution for the control containing solely iron. 1mL each of 8mM copper(II) and ferrous solutions were added for the control containing iron and copper.

III.2 Characterization.

Scanning electron microscopy (SEM) was performed using a FEI Sirion XL30 with electron dispersive spectroscopy (EDS, Oxford). Transmission electron microscopy (TEM) was performed using FEI Tecnai G2 F20 with 200 kV accelerating voltage. Samples for TEM were prepared by dropping a dispersion of nanowires onto a silicon nitride membrane (50 nm thick, Ted Pella, Inc.) and immediately evaporating the solvent at 50°C.

Xray Diffraction (XRD) was performed on a Bruker D8 Discover with GADDS XRD system with averaged Cu K-alpha radiation source. Samples were aligned in the system using the laser guidance system provided in the instrument.

Dynamic Light Scattering (DLS) measurements were performed to measure the size and zeta potential (surface charge) of suspended Palladium nanoparticles using a Malvern Instruments Zetasizer NanoZS equipped with a 633nm HeNe laser operating at a scattering angle of 173° (backscattering setup).

X-ray photoelectron spectroscopy (XPS) was performed using a PHI 5000 VersaProbe setup using Al Ka radiation. Acquired spectra were deconvolved and analyzed with PHI MultiPak software (Physical Electronics, Chanhassen, MN). The energy calibrations were made against the C1s peak (284.8 eV) of adventitious carbon as a reference. Powder samples were aligned in the system using the laser guidance system provided in the instrument.
Neutron activation analysis (NAA) was performed using a TRIGA Mark II Nuclear Reactor. The samples of approximately 1mg of dried Palladium nanowires were irradiated for 30 minutes operating at 100 kW thermal power, $4x10^{12}$ neutrons/cm^2*sec thermal flux and $4.8x10^{12}$ neutrons/cm^2*sec fast and epithermal flux. Samples were counted while positioned near the surface of a 25cm^2, trapezohedral, germanium, lithium-drifted semiconductor detector (Nuclear Diodes), which is constantly cooled by liquid nitrogen (77°K). Dead time between end of

irradiation and start of collection was 19 hours 18 minutes. Detection of copper was monitored for the decay of ^{65}Cu to ^{64}Cu at characteristic energy 1345 keV, half-life 12.7 hours. Detection of palladium was monitored for the decay from ^{109}Pd to ^{109m}Ag at the characteristic energy 88keV, half-life 13.7 hours. The counts per second (cps) for Palladium and Copper $4.567x10^{05}$ and $7.5019x10^{-002}$ respectively. After accounting for detector efficiency, these counts correspond to activities of $1.1856x10^{08}$ and 818.3147uCi. From the activity counts the number of number of product atoms produced for a stable product could be predicted from:

$$N^* = N\Phi\sigma t$$

Where:

N* = the number of product atoms

N = the number of target atoms

Φ = neutron flux - (neutrons/cm^2*sec)

σ = cross-section (cm^{-2})

t = time in detector (sec)

Given that unstable products begin to decay as soon as they are produced, a correction factor is introduced into the above equation. As activation time increases, the amount of unstable product increases, as does its rate of decay. This is accounted for with a saturation factor:

$$dN^*/dt = N\Phi\sigma t(-\lambda N^*)$$

$$\lambda N^* = N\Phi\sigma t[1 - \exp(-0.693 t_i / t_{1/2})]$$

$$= N\Phi\sigma t^*[\text{saturation factor}]$$

Where:

t_i = irradiation time (sec)

$t_{1/2}$ = half-life of product (sec)

III. Results and Discussion:

Palladium nanowires with extremely long (10+ um), high aspect ratios (>500) and have been synthesized hydrothermally utilizing a trace amount of copper. Controls were performed varying the copper concentration and time of experiment to optimize wire growth. The concentration of copper is varied between 8nM and 8 mM, yielding a final copper concentration range between 0.666 nM and 0.666 mM. This corresponds to a Pd/Cu atomic ratio ranging from 12.5 to 12.5 million. Optimal wire growth was obtained with initial solutions of 8uM copper. Concentrations above and below this produced wires of significantly lower aspect ratio and submicron length. Temporal experiments were performed as well, varying hydrothermal dwell time from 2 to 24 hours. Wire lengths increased with time to up to 10 hours and then remained constant.

Control experiments using no trace metals produced similar results with the majority of particles of submicron length and few 1-2um wires (fig 7). Thus copper plays a definite role in wire growth. A potential role for the copper would be to act as a sacrificial lamb in oxidative etching. The rate of oxidation of metallic (Pd0) to the ion Pd(II) occurs selectively along high energy crystalline planes - retarding growth of FCC palladium along the {111} direction. Ferrous ions act as additional oxidizing agents to further enhance the role of native oxidizing agents in solution such as dissolved oxygen. Controls using ferrous solutions were performed to examine the role of copper in the synthesis with respect to oxidative etching. With the addition of solely ferrous ions to solution prevented all wire growth producing submicron cubic and ellipsoidal particles. The addition of copper and ferrous ions produced ellipsoidal particles and submicron nanorods. Thus copper was able to partially prevent oxidative etching, allowing for growth of one dimensional nanorods. Furthermore this highlights the delicate balance of copper to oxidative species present in the reaction and growth mechanism.

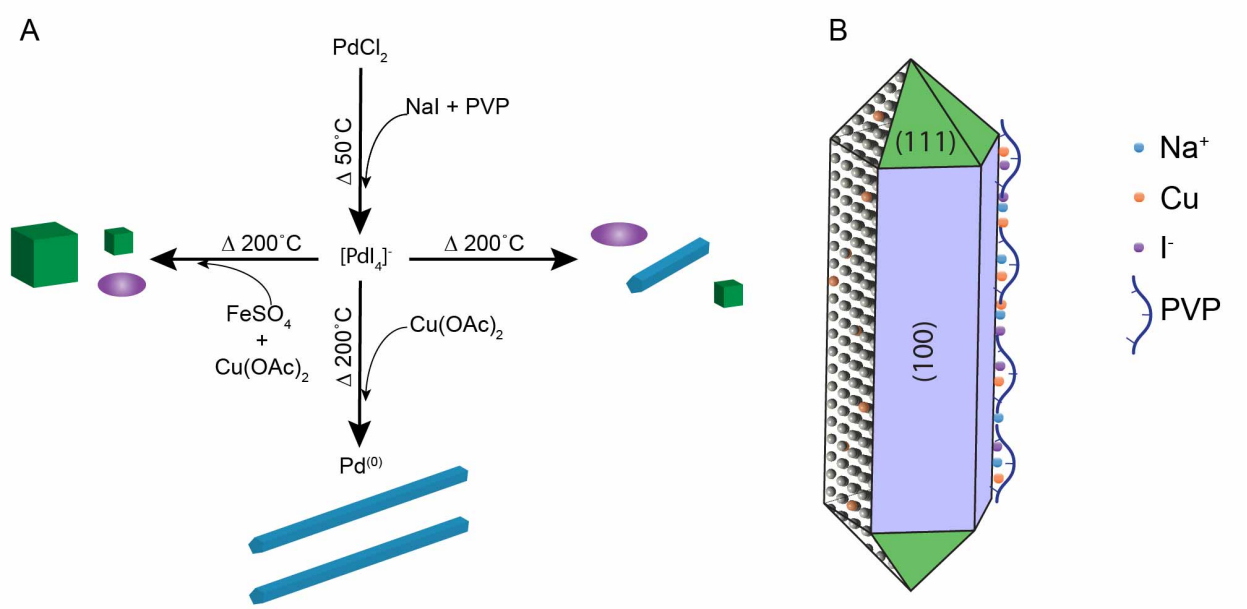

FIGURE 7 | Synthesis of Palladium Nanowires

a) Reaction Pathway of Palladium nanowire synthesis consisting of an initial palladium iodate complex precursor followed by trace metal addition and hydrothermal reaction with 10 hour dwell time.

b) Schematic of Palladium nanowire with [100] growth direction and surface coatings

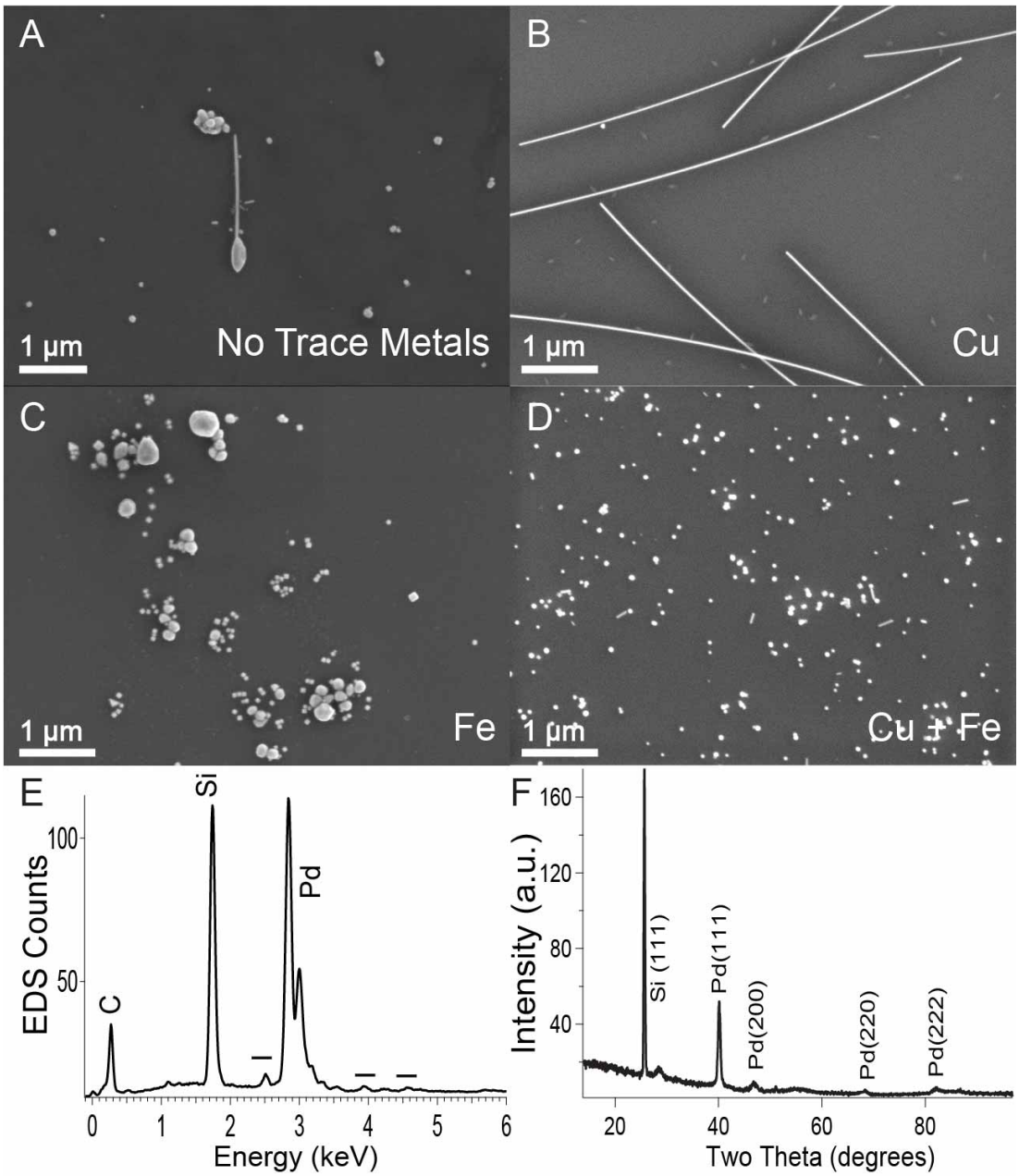

FIGURE 8 | Physical Characterization

(a-d) Scanning electron microscope images of palladium nanoparticles synthesized without trace metals (a), with 8uM copper(II) addition (b), 8 uM iron(II) addition, and 8uM additions of both copper(II) and iron(II) (d). Scale bar = 1 um.

e) SEM energy dispersive spectroscopy (EDS) spectra of Palladium nanowires synthesized with 8uM copper(II) indicating carbon and iodine presence. (Pd 38.46%, C 21.51%, Si 38.32%, I 1.51%).

f) Xray diffraction (XRD) of Palladium nanowires synthesized with 8uM copper(II) indicating enrichment of (111) and (100) crystal planes. Silicon (111) peak is from the silicon wafer substrate.

Further characterization was performed to quantify the physical dimensionality and distributions of the nanoparticles. Dynamic light scattering (DLS) is a bulk measurement to determine the particle size distribution (PSD) and zeta potential (surface charge) of NP suspensions. The intensity PSD is a first order result, weighted scattering intensity of each particle fraction or family. Small aggregations and larger particles dominate the intensity PSD such that it is a sensitive detector for larger particles such as nanowires [48]. The volume distribution, calculated from the intensity distribution using Mie theory, is used to estimate relative proportions from multiple peaks [48]. While the theory assumes spherical morphologies, the relative radii of long, large nanowires verses the smaller NPs are easily distinguishable. PSD values for NPs synthesized with suboptimal copper concentrations as well as control experiments confirm smaller NPs with submicron hydrodynamic radii (table 1). PSD values for nanowires synthesized with 8uM copper concentration show a significantly greater population (74.9%) of nanoparticles with hydrodynamic radii over a micron. SEM was utilized to quantify lengths and aspect ratios of particle distributions (table 2). The average length of nanoparticles for suboptimal copper syntheses was similar with 150nm (n=50) with large standard deviations. The average length of wires at optimal copper concentration was 9.0um with standard deviation 2.6um. The nanowires appear remarkably malleable and often have a curvature or are bent.

Zeta potential, the potential difference between the dispersion medium and the stationary layer of fluid attached to the dispersed particle, is a measure of stability of particle dispersion and stability with large magnitudes (>10mV) indicating stability. Zeta potential for all syntheses (see table 1) is close to zero, indicating low surface charge of the Palladium nanowires and relative instability. Steric and charge stabilization from adsorption of the PVP polymer coating likely confers stability and dispersability to the nanowires as seen through DF and visually[49].

Concentration	Intensity PSD (d.nm)	Volume PSD (d.nm)	Zeta Potential (mV)
No Cu	205.1 ± 64.27 (100)	238.2 ± 76.03	-5.05 ± 6.04
8 nM	1189 ± 394.3 (66.7) 220.9 ± 56.96 (19.6) 5148 ± 517.0 (13.7)	5267 ± 724.7 (61.6) 1270 ± 482.8 (35.8) 246.3 ± 64.03 (2.5)	4 ± 5.13
80 nM	205.7 ± 79.40 (99.0) 4969 ± 622.6 (1.0)	253.6 ± 100.1 (73.9) 5134 ± 782.1 (26.1)	-6.99 ± 5.32
800 nM	233.5 ± 106.5 (97.4) 4758 ± 744.8 (2.6)	308.4 ± 134.8 (60.4) 4988 ± 854.2 (39.6)	1.64 ± 4.99
8 uM	1516 ± 878.5 (74.9) 235.5 ± 87.26 (25.1)	2009 ± 1212 (100)	2.71 ± 4.3
80 uM	140.3 ± 49.26 (100)	99.11 ± 26.31 (57.3) 195.6 ± 46.56 (42.7)	-8.27 ± 8.53
800 uM	146.6 ± 57.95 (98.6) 28.56 ± 4.482 (1.4)	199.0 ± 61.10 (36.2) 85.92 ± 22.62 (32.6) 26.91 ± 5.232 (31.2)	-7.32 ± 7.94
8 mM	147.9 ± 52.20 (100)	190.8 ± 55.85 (59.0) 94.50 ± 19.94 (41.0)	-2.97 ± 7.13
Fe	237.3 +/- 75.03	206.5 +/- 72.20	-12.0 +/- 7.70
Fe + Cu	425.9 +/- 127.3	375.6 +/- 118.7	-16.6 +/- 7.71

TABLE 1 | Dynamic Light Scattering and Zeta Potential
Intensity and volume particle size distributions (PSDs) of PalladiumNP hydrodynamic diameters (nm) synthesized with 1mL of trace metal solution of varying concentration and corresponding zeta potential (mV). Weight percent per radii range is in parenthesis.

Concentration	Major Axis (nm)	Aspect Ratio
No Cu	162 +/- 67	1.57 +/- 0.68
8 nm	172 +/- 62	1.58 +/- 0.68
80 nm	169 +/- 44	1.55 +/- 0.53
800 nm	223+/- 110	1.74 +/- 1.86
8 um	8960 +/- 2601	448 +/- 130
80 um	130 +/- 30	1.17 +/- 0.13
800 um	134 +/- 38	1.37 +/- 0.46
8 mm	110 +/- 67	2.10 +/- 1.75
Fe	218 +/- 90	1.37 +/- 0.62
Fe and Cu	396 +/- 148	1.62 +/- 0.41

TABLE 2 | Particle Size Distribution Analysis
Particle major axis lengths and aspect ratios measured from SEM images. Sample size 100 particles.

XRD was used to ascertain the face centered cubic (FCC) nature of the crystals (fig 7.f). Peaks with two theta values 40.1, 46.7, and 68.1 degrees correspond to the 111, 200, and 220 peaks respectively according to literature. Intensity values for FCC palladium are 68298.7:32474.3:19706.0:23459.0:6949.4 for 111:200:220:113:222 planes (WWW-MINCRYST, card 3428).. From fig 7.f there is significant deviation from this ratio indicative of texturing from both the <111> and <110> planes of the pentagonal wire geometry.

TEM spectroscopy detailed the crystalline twinned nature of the particles with bright field (BF) images (fig 9.a,b). The wires are highly ductile and easily adhere to the substrate with large degrees of curvature (fig 9.a). Bragg diffraction spots (fig 9.b) are visible throughout the wires. The PVP coating is present as a 3-5nm coating (fig 11).

Structural and chemical compositions were further examined via TEM. High angle annular-dark-field (HAADF) confirmed the presence of Copper throughout the wire with potential selective copper enrichment along the wire edge (fig 9.c). Select area electron diffraction (SAED) confirmed the FCC nature of the nanowires. Additional 100, 101, and 112 peaks with respective d-spacings of 3.67, 2.72, and 1.59 Angstroms were identified as well (fig 9.3). These are FCC-forbidden Bragg reflections as the hkl values contain both even and odd. These peaks are not present in XRD and could represent a face-centered-tetragonal (FCT) phase. They do not match known bimetallic palladium copper alloys including PdCu, PdCu3, and Pd3Cu or NaI, PdI, CuI complexes that could form from surface iodine remnants. SAED of a single nanowire (fig. 10) reveals a complex diffraction pattern, reaffirming crystallinity of the wire as well as indicating a complex structure due to the twinning.

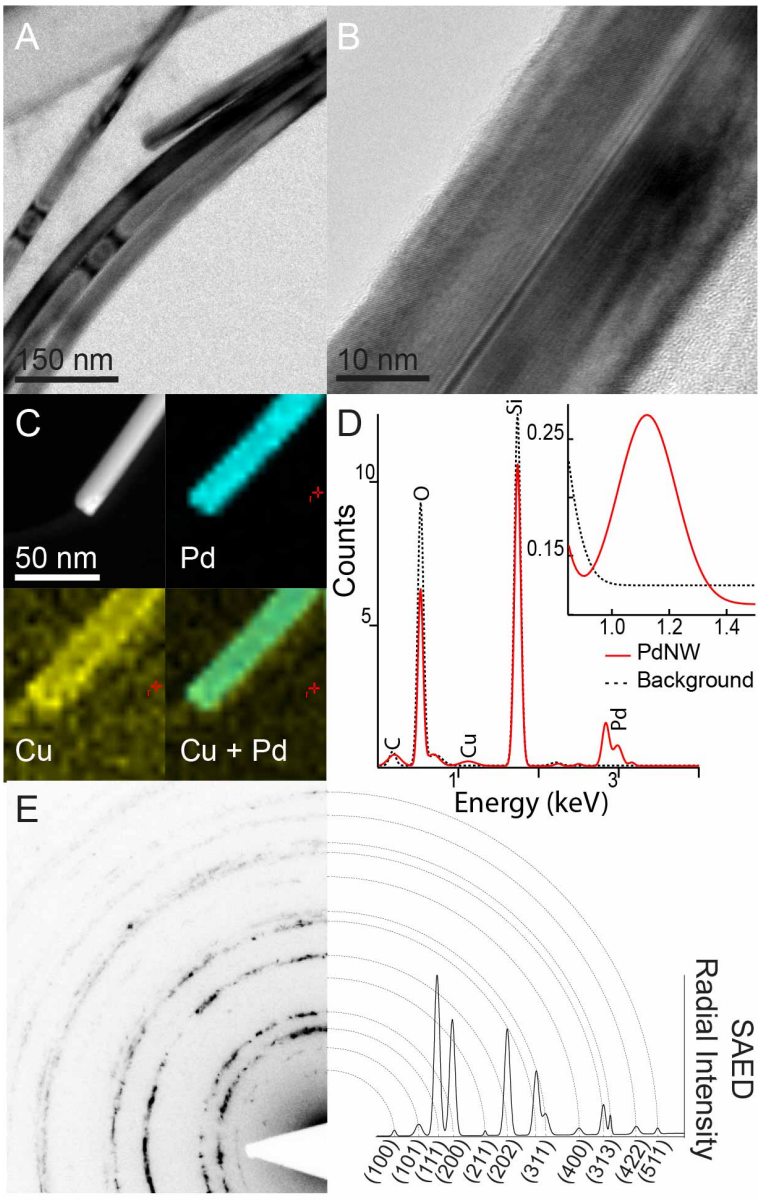

FIGURE 9 | Transmission Electron Microscopy

a) Bright field transmission electron microscope image of Palladium nanowires; scale bar = 150nm.

b) Bright field transmission electron microscope of an individual Palladium nanowire; scale bar = 10nm.

c) High angle annular-dark-field (HAADF) image of a Palladium nanowire showing copper enrichment along the wire; scale bar = 50nm.

d) TEM-EDS spectra of a Palladium nanowire (red) and background SiO_2 grid (black) showing 1% Copper composition.

e) Select area electron diffraction of cluster of Palladium nanowires suggesting presence of non-fcc phase present due to (001), (101), and (112) peaks.

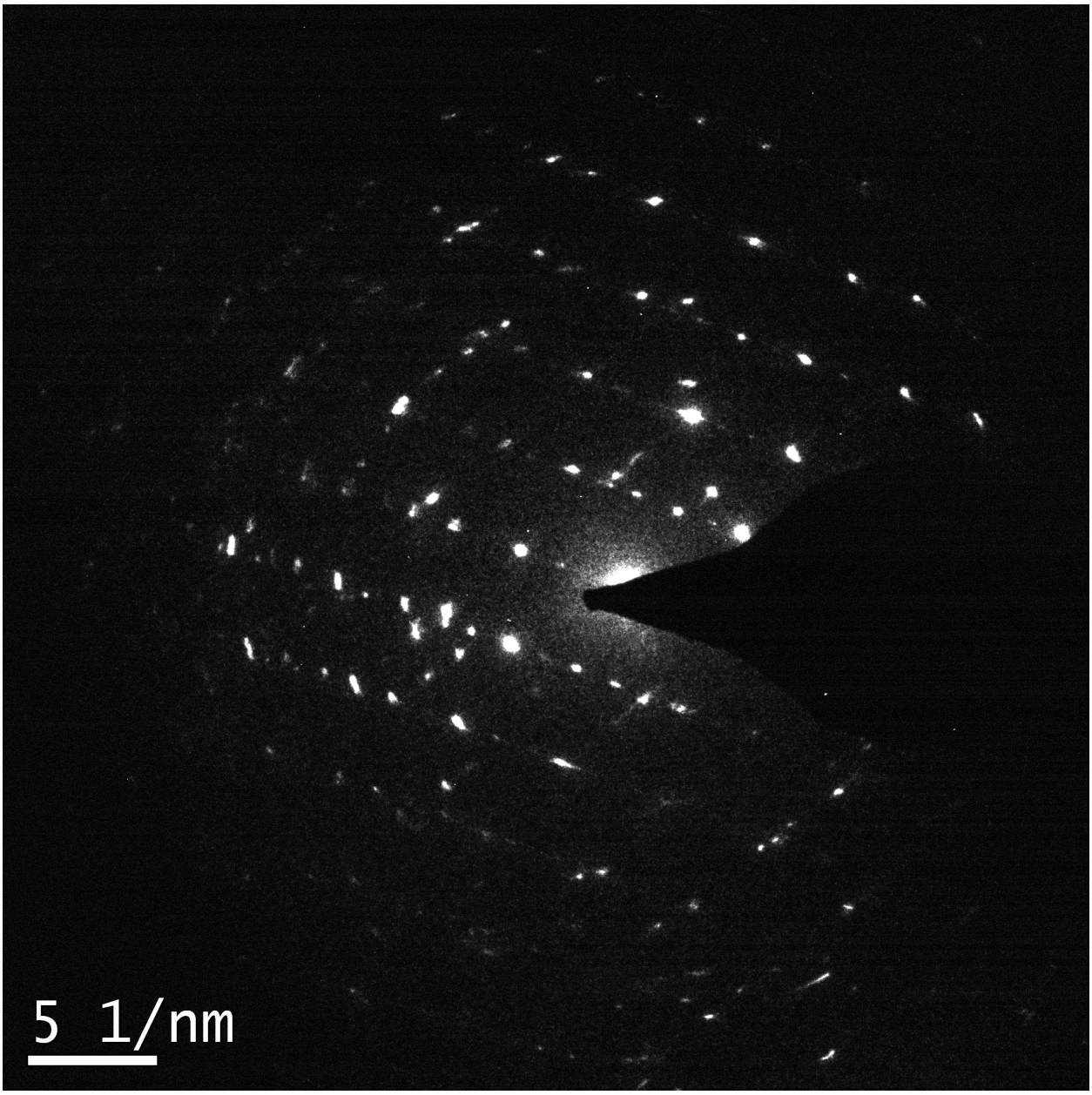

FIGURE 10 | Select Area Electron Diffraction
Select area electron diffraction of a single Palladium nanowire suggesting complex twinning crystalline nature of the wire.

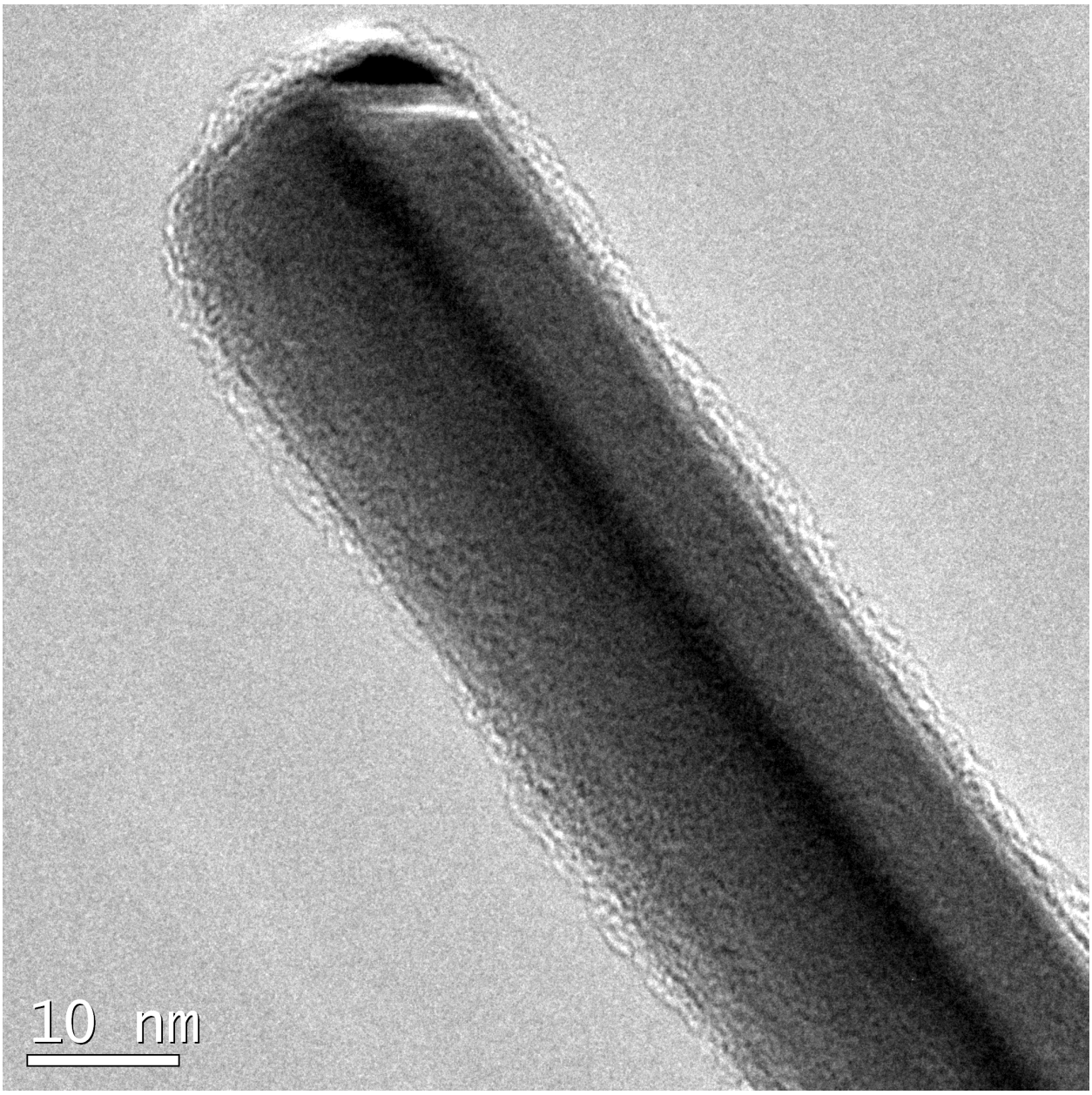

FIGURE 11 | Select Area Electron Diffraction
Bright field transmission electron microscope image of a single Palladium nanowire detailing surface coating; scale bar = 10nm.

TEM and SEM-EDS, NAA, and XPS were utilized to ascertain the chemical composition of the nanowires. TEM-EDS was used to quantitatively determine the percent copper and Pd/Cu ratios ultimately found in the nanowires. Electron dispersive spectroscopy (EDS) spectra quantified 1% Copper composition (fig 9.d). The detection limit is 1000ppm or 0.1 at% under optimal operating conditions [50]. SEM-EDS confirms the presence of iodine (1.51%) and carbon (21.5%) from the PVP coating (fig 7.e). Copper was not above the detection limit of approximately between 0.5 and 1at% under optimal operating conditions [51][52].

Neutron activation analysis is a quantitative method in which neutron-activated radioactive samples are monitored via gamma decay counts for elemental identification[53]. Palladium and copper quantities were measured by this technique (fig 12.a). Copper was monitored via activation of the ^{63}Cu by the reaction (n,Y) giving the radioisotope ^{64}Cu with half-life $T_{1/2}$=12.74 h and characteristic energy 1345keV[54][55][56]. Palladium was monitored for the decay from ^{109}Pd to ^{109m}Ag at the characteristic energy 88keV, half-life $T_{1/2}$=13.7 hours. ^{109}Pd undergoes beta decay to ^{109}Ag via $^{108}Pd(n,Y)^{109}Pd(B-)^{109}Ag^{m}$ with most beta decay going directly to the metastable state $^{109}Ag^{m}$ that undergoes complete gamma decay to the stable ground state ^{109}Ag[57][58]. The activities for Palladium and Copper 1.1856E+08 and 818.3147 uCi respectively, correlating to a Pd/Cu ratio of 16000:1 or 0.0062 at% Cu or 62ppm Cu.

X-ray Photoelectron spectroscopy (XPS) was performed to ascertain surface chemical composition. Palladium nanowire samples were treated with oxygen plasma to expose the metallic surface, removing the majority of PVP polymer coating. Carbon (C1S 284eV), sodium (Na1S 1070.5eV), iodine (I3p3/2, 876eV), and palladium (Pd3d3/2 335.5, Pd3p3/2 532.5, Pd3p1/2 561 eV) peaks are present in the spectra (fig 12.b)[59][60][61][62][63][64]. Partial oxidation can be seen through double peaks for metallic and oxidized state of the iodine I3d5/2 (619, 623 eV) and I3d3/2 (630.5, 635 ev). An additional Silicon substrate peak is visible as well.

The presence of copper remains indeterminate. A potential copper 2p3/2 peak (expected 932eV)[65] overlaps directly with a prominent Iodine 3p3/2 peak (also at 932 eV). The iodine peak (fig 12.b inset) has a bulge suggestive of trace copper. Given the trace amounts of copper used in the synthesis, the other peak of the copper 3p doublet would be under the signal to noise as well.

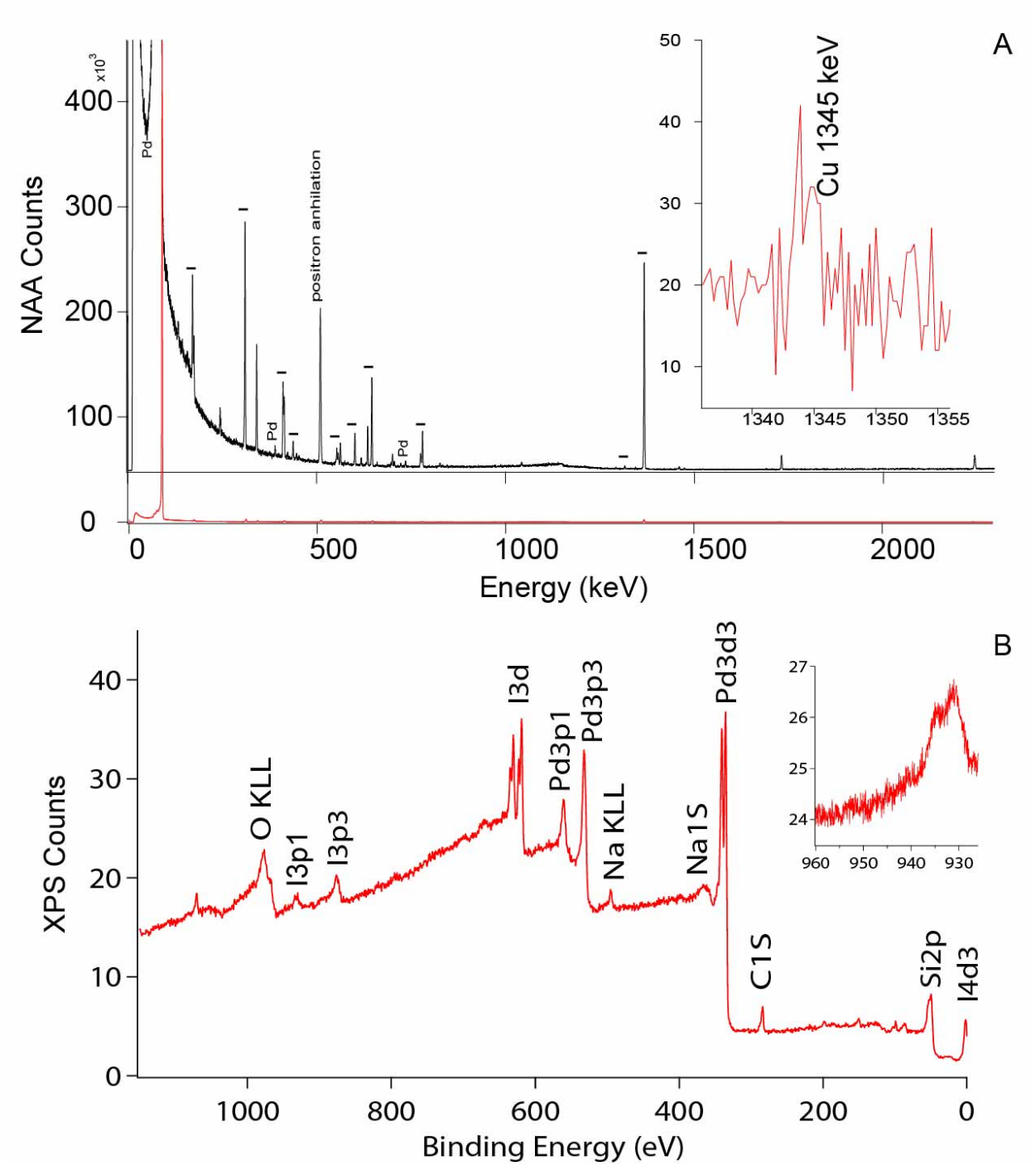

FIGURE 12 | Chemical Characterization

a) Neutron activation analysis (NAA) of Palladium nanowires presenting a prominent Palladium peak at 88keV and copper peak at 1345 keV (inset).

b) Xray photoelectron spectroscopy (XPS) of Palladium nanowire dispersion on Silicon substrate presenting prominent sodium and iodine peaks. Prominent Iodine 3p3/2 binding energy at 932 eV overlaps with potential copper 2p3/2 peak (expected 932eV) (inset).

V. Conclusions:

Palladium nanowires of remarkably high aspect ratio have been synthesized using a specific trace amount of copper. Through neutron activation analysis (NAA) and transmission electron microscopy electron dispersive energy (TEM-EDS) the copper content in the wires is between 62ppm and 1000ppm. SEM-EDS and XPS suggest that sodium, iodine, and organic poly-vinylpyrrolidone coat the surface. Further work is underway to ascertain the spatial location of copper throughout the wires to ascertain if copper preferentially aggregates along twinning planes or the surface.

ACKNOWLEDGEMENTS:

This research was supported in part by a grant from the American Chemical Society's Petroleum Research Fund. The author would like to thank Xuezhe Zhou, Frances Hocutt and Zach Rousslang for valuable discussion as well as professors Dwayne Arola and Kannan Krishnan for invaluable feedback. Most of all, many thanks to Professor Peter Pauzauskie for support and guidance.

REFERENCES:

[1] F. Yang, D. Jung, and R. M. Penner, "Trace Detection of Dissolved Hydrogen Gas in Oil Using a Palladium Nanowire Array," *Anal. Chem.*, vol. 83, no. 24, pp. 9472–9477, Dec. 2011.

[2] F. Yang, S.-C. Kung, M. Cheng, J. C. Hemminger, and R. M. Penner, "Smaller is Faster and More Sensitive: The Effect of Wire Size on the Detection of Hydrogen by Single Palladium Nanowires," *ACS Nano*, vol. 4, no. 9, pp. 5233–5244, Sep. 2010.

[3] R. Long, K. Mao, X. Ye, W. Yan, Y. Huang, J. Wang, Y. Fu, X. Wang, X. Wu, Y. Xie, and Y. Xiong, "Surface Facet of Palladium Nanocrystals: A Key Parameter to the Activation of Molecular Oxygen for Organic Catalysis and Cancer Treatment," *J. Am. Chem. Soc.*, vol. 135, no. 8, pp. 3200–3207, Feb. 2013.

[4] Z. A. Chase, J. L. Fulton, D. M. Camaioni, D. Mei, M. Balasubramanian, V.-T. Pham, C. Zhao, R. S. Weber, Y. Wang, and J. A. Lercher, "State of Supported Pd during Catalysis in Water," *J. Phys. Chem. C*, vol. 117, no. 34, pp. 17603–17612, Aug. 2013.

[5] W. W. Webb, "Dislocation Mechanisms in the Growth of Palladium Whisker Crystals," *J. Appl. Phys.*, vol. 36, no. 1, pp. 214–221, Jan. 1965.

[6] Y. Yoo, I. Yoon, H. Lee, J. Ahn, J.-P. Ahn, and B. Kim, "Pattern-Selective Epitaxial Growth of Twin-Free Pd Nanowires from Supported Nanocrystal Seeds," *ACS Nano*, vol. 4, no. 5, pp. 2919–2927, May 2010.

[7] A. R. Halpern, N. Nishi, J. Wen, F. Yang, C. Xiang, R. M. Penner, and R. M. Corn, "Characterization of Electrodeposited Gold and Palladium Nanowire Gratings with Optical Diffraction Measurements," *Anal. Chem.*, vol. 81, no. 14, pp. 5585–5592, Jul. 2009.

[8] O. Corduneanu, V. C. Diculescu, A.-M. Chiorcea-Paquim, and A.-M. Oliveira-Brett, "Shape-controlled palladium nanowires and nanoparticles electrodeposited on carbon electrodes," *J. Electroanal. Chem.*, vol. 624, no. 1–2, pp. 97–108, Dec. 2008.

[9] C. Koenigsmann, A. C. Santulli, E. Sutter, and S. S. Wong, "Ambient Surfactantless Synthesis, Growth Mechanism, and Size-Dependent Electrocatalytic Behavior of High-Quality, Single Crystalline Palladium Nanowires," *ACS Nano*, vol. 5, no. 9, pp. 7471–7487, Sep. 2011.

[10] K. Kim, M. Kim, and S. M. Cho, "Pulsed electrodeposition of palladium nanowire arrays using AAO template," *Mater. Chem. Phys.*, vol. 96, no. 2–3, pp. 278–282, Apr. 2006.

[11] K. J. Jeon, J. M. Lee, E. Lee, and W. Lee, "Individual Pd nanowire hydrogen sensors fabricated by electron-beam lithography," *Nanotechnology*, vol. 20, no. 13, p. 135502, Apr. 2009.

[12] B. Lim, M. Jiang, J. Tao, P. H. C. Camargo, Y. Zhu, and Y. Xia, "Shape-Controlled Synthesis of Pd Nanocrystals in Aqueous Solutions," *Adv. Funct. Mater.*, vol. 19, no. 2, pp. 189–200, Jan. 2009.

[13] J. Yoon, N. T. Khi, H. Kim, B. Kim, H. Baik, S. Back, S. Lee, S.-W. Lee, S. J. Kwon, and K. Lee, "High yield synthesis of catalytically active five-fold twinned Pt nanorods from a surfactant-ligated precursor," *Chem. Commun.*, vol. 49, no. 6, pp. 573–575, Dec. 2012.

[14] V. La Ferrara, B. Alfano, E. Massera, and G. Di Francia, "Single palladium nanowire growth in place assisted by dielectrophoresis and focused ion beam," *J. Nanosci. Nanotechnol.*, vol. 9, no. 5, pp. 2931–2936, May 2009.

[15] X. Huang and N. Zheng, "One-Pot, High-Yield Synthesis of 5-Fold Twinned Pd Nanowires and Nanorods," *J. Am. Chem. Soc.*, vol. 131, no. 13, pp. 4602–4603, Apr. 2009.

[16] K. E. Korte, S. E. Skrabalak, and Y. Xia, "Rapid synthesis of silver nanowires through a CuCl- or CuCl2-mediated polyol process," *J. Mater. Chem.*, vol. 18, no. 4, pp. 437–441, Jan. 2008.
[17] D. W. Oxtoby, "Phase transitions: Catching crystals at birth," *Nature*, vol. 406, no. 6795, pp. 464–465, Aug. 2000.
[18] Y. Xiong and Y. Xia, "Shape-Controlled Synthesis of Metal Nanostructures: The Case of Palladium," *Adv. Mater.*, vol. 19, no. 20, pp. 3385–3391, Oct. 2007.
[19] A. R. Tao, S. Habas, and P. Yang, "Shape Control of Colloidal Metal Nanocrystals," *Small*, vol. 4, no. 3, pp. 310–325, Mar. 2008.
[20] S. Auer and D. Frenkel, "Prediction of absolute crystal-nucleation rate in hard-sphere colloids," *Nature*, vol. 409, no. 6823, pp. 1020–1023, Feb. 2001.
[21] U. Gasser, E. R. Weeks, A. Schofield, P. N. Pusey, and D. A. Weitz, "Real-Space Imaging of Nucleation and Growth in Colloidal Crystallization," *Science*, vol. 292, no. 5515, pp. 258–262, Apr. 2001.
[22] A. C. Hillier and M. D. Ward, "Atomic Force Microscopy of the Electrochemical Nucleation and Growth of Molecular Crystals," *Science*, vol. 263, no. 5151, pp. 1261–1264, Mar. 1994.
[23] Z. Zhang and M. G. Lagally, "Atomistic Processes in the Early Stages of Thin-Film Growth," *Science*, vol. 276, no. 5311, pp. 377–383, Apr. 1997.
[24] S.-T. Yau and P. G. Vekilov, "Quasi-planar nucleus structure in apoferritin crystallization," *Nature*, vol. 406, no. 6795, pp. 494–497, Aug. 2000.
[25] V. K. LaMer and R. H. Dinegar, "Theory, Production and Mechanism of Formation of Monodispersed Hydrosols," *J. Am. Chem. Soc.*, vol. 72, no. 11, pp. 4847–4854, 1950.
[26] J.-M. Zhang, F. Ma, and K.-W. Xu, "Calculation of the surface energy of FCC metals with modified embedded-atom method," *Appl. Surf. Sci.*, vol. 229, no. 1–4, pp. 34–42, May 2004.
[27] D. J. Smith, A. K. Petford-Long, L. R. Wallenberg, and J.-O. Bovin, "Dynamic Atomic-Level Rearrangements in Small Gold Particles," *Science*, vol. 233, no. 4766, pp. 872–875, Aug. 1986.
[28] J. L. Elechiguerra, J. Reyes-Gasga, and M. J. Yacaman, "The role of twinning in shape evolution of anisotropic noble metal nanostructures," *J. Mater. Chem.*, vol. 16, no. 40, p. 3906, 2006.
[29] P. L. Gai and M. A. Harmer, "Surface Atomic Defect Structures and Growth of Gold Nanorods," *Nano Lett.*, vol. 2, no. 7, pp. 771–774, 2002.
[30] C. Lofton and W. Sigmund, "Mechanisms Controlling Crystal Habits of Gold and Silver Colloids," *Adv. Funct. Mater.*, vol. 15, no. 7, pp. 1197–1208, 2005.
[31] F. Baletto and R. Ferrando, "Structural properties of nanoclusters: Energetic, thermodynamic, and kinetic effects," *Rev. Mod. Phys.*, vol. 77, no. 1, pp. 371–423, May 2005.
[32] C. J. Murphy, T. K. Sau, A. M. Gole, C. J. Orendorff, J. Gao, L. Gou, S. E. Hunyadi, and T. Li, "Anisotropic Metal Nanoparticles: Synthesis, Assembly, and Optical Applications," *J. Phys. Chem. B*, vol. 109, no. 29, pp. 13857–13870, Jul. 2005.
[33] B. Wiley, T. Herricks, Y. Sun, and Y. Xia, "Polyol Synthesis of Silver Nanoparticles: Use of Chloride and Oxygen to Promote the Formation of Single-Crystal, Truncated Cubes and Tetrahedrons," *Nano Lett.*, vol. 4, no. 9, pp. 1733–1739, Sep. 2004.

[34] Y. Xiong, J. Chen, B. Wiley, Y. Xia, S. Aloni, and Y. Yin, "Understanding the Role of Oxidative Etching in the Polyol Synthesis of Pd Nanoparticles with Uniform Shape and Size," *J. Am. Chem. Soc.*, vol. 127, no. 20, pp. 7332–7333, 2005.
[35] G. Rupprechter and C. Weilach, "Mind the gap! Spectroscopy of catalytically active phases," *Nano Today*, vol. 2, no. 4, pp. 20–29, Aug. 2007.
[36] C. C. C. Johansson Seechurn, M. O. Kitching, T. J. Colacot, and V. Snieckus, "Palladium-Catalyzed Cross-Coupling: A Historical Contextual Perspective to the 2010 Nobel Prize," *Angew. Chem. Int. Ed.*, vol. 51, no. 21, pp. 5062–5085, 2012.
[37] T. Mizoroki, K. Mori, and A. Ozaki, "Arylation of Olefin with Aryl Iodide Catalyzed by Palladium," *Bull. Chem. Soc. Jpn.*, vol. 44, no. 2, pp. 581–581, 1971.
[38] N. Miyaura and A. Suzuki, "Palladium-Catalyzed Cross-Coupling Reactions of Organoboron Compounds," *Chem. Rev.*, vol. 95, no. 7, pp. 2457–2483, 1995.
[39] K. Sonogashira, "Development of Pd–Cu catalyzed cross-coupling of terminal acetylenes with sp2-carbon halides," *J. Organomet. Chem.*, vol. 653, no. 1–2, pp. 46–49, Jul. 2002.
[40] Y. Hatanaka and T. Hiyama, "Cross-coupling of organosilanes with organic halides mediated by a palladium catalyst and tris(diethylamino)sulfonium difluorotrimethylsilicate," *J. Org. Chem.*, vol. 53, no. 4, pp. 918–920, 1988.
[41] R. F. Heck and J. P. Nolley, "Palladium-catalyzed vinylic hydrogen substitution reactions with aryl, benzyl, and styryl halides," *J. Org. Chem.*, vol. 37, no. 14, pp. 2320–2322, 1972.
[42] F. D. Manchester, A. San-Martin, and J. M. Pitre, "The H-Pd (hydrogen-palladium) System," *J. Phase Equilibria*, vol. 15, no. 1, pp. 62–83, Feb. 1994.
[43] W. Grochala and P. P. Edwards, "Thermal Decomposition of the Non-Interstitial Hydrides for the Storage and Production of Hydrogen," *Chem. Rev.*, vol. 104, no. 3, pp. 1283–1316, Mar. 2004.
[44] J. Henriksson, L. G. Villanueva, and J. Brugger, "Ultra-low power hydrogen sensing based on a palladium-coated nanomechanical beam resonator," *Nanoscale*, vol. 4, no. 16, pp. 5059–5064, Jul. 2012.
[45] T. Mitsui, M. K. Rose, E. Fomin, D. F. Ogletree, and M. Salmeron, "Dissociative hydrogen adsorption on palladium requires aggregates of three or more vacancies," *Nature*, vol. 422, no. 6933, pp. 705–707, Apr. 2003.
[46] N. Lopez, Z. Łodziana, F. Illas, and M. Salmeron, "When Langmuir Is Too Simple: H2 Dissociation on Pd(111) at High Coverage," *Phys. Rev. Lett.*, vol. 93, no. 14, p. 146103, Sep. 2004.
[47] J. E. Worsham Jr., M. K. Wilkinson, and C. G. Shull, "Neutron-diffraction observations on the palladium-hydrogen and palladium-deuterium systems," *J. Phys. Chem. Solids*, vol. 3, no. 3–4, pp. 303–310, 1957.
[48] B. E. Dahneke, *Measurement of suspended particles by quasi-elastic light scattering*. Wiley, 1983.
[49] G. M. Dougherty, K. A. Rose, J. B.-H. Tok, S. S. Pannu, F. Y. S. Chuang, M. Y. Sha, G. Chakarova, and S. G. Penn, "The zeta potential of surface-functionalized metallic nanorod particles in aqueous solution," *ELECTROPHORESIS*, vol. 29, no. 5, pp. 1131–1139, Mar. 2008.
[50] D. B. Williams and B. C. Carter, *Transmission Electron Microscopy*, 2nd ed. Springer US, 2009.
[51] A. Pintar, J. Batista, and I. Muševič, "Palladium-copper and palladium-tin catalysts in the liquid phase nitrate hydrogenation in a batch-recycle reactor," *Appl. Catal. B Environ.*, vol. 52, no. 1, pp. 49–60, Sep. 2004.

[52] *Scanning Electron Microscopy and X-ray Microanalysis: Third Edition*. Springer US, 2003.
[53] D. De Soete, R. Gijbels, and J. Hoste, *Neutron activation analysis*, 1st ed. New York, NY: John Wiley and Sons, 1972.
[54] M. Ebihara, S. Fukatsu, K. Hirano, and H. Ozaki, "Neutron activation analysis of trace copper, zinc and indium in geological and meteoritic samples, using rapid chemical separations," *J. Radioanal. Nucl. Chem.*, vol. 182, no. 2, pp. 295–303, Aug. 1994.
[55] A. Olariu, "Neutron activation analysis of some Neolithic copper objects," *ArXivnucl-Ex9908023*, Aug. 1999.
[56] G. S. Fell, H. Smith, and R. A. Howie, "Neutron activation analysis for copper in biological material applied to Wilson's disease," *J. Clin. Pathol.*, vol. 21, no. 1, pp. 8–11, Jan. 1968.
[57] I. Ahmad, S. Ahmad, and D. F. C. Morris, "Determination of noble metals in geological materials by radiochemical neutron-activation analysis," *Analyst*, vol. 102, no. 1210, pp. 17–24, Jan. 1977.
[58] L. G. Cilindro and D. S. M. Jr, "Neutron activation analysis for iridium, palladium and silver in platinum," *J. Radioanal. Chem.*, vol. 3, no. 3–4, pp. 195–204, Sep. 1969.
[59] P. Steiner, F. J. Reiter, H. Höchst, S. Hüfner, and J. C. Fuggle, "Lineshape of the KL2L3(1D2) Auger line in magnesium and sodium metal," *Phys. Lett. A*, vol. 66, no. 3, pp. 229–232, May 1978.
[60] H. Moers, J. G. Dillard, H. Klewe-Nebenius, G. Kirch, G. Pfennig, and H. J. Ache, "XPS study of iodine released in core melting experiments," *Surf. Interface Anal.*, vol. 7, no. 1, pp. 22–28, Feb. 1985.
[61] J. G. Dillard, H. Moers, H. Klewe-Nebenius, G. Kirch, G. Pfennig, and H. J. Ache, "X-ray photoelectron and Auger electron spectroscopic study of the adsorption of molecular iodine on uranium metal and uranium dioxide," 1984.
[62] J. P. Mathew and M. Srinivasan, "Photoelectron spectroscopy (XPS) studies on some palladium catalysts," *Eur. Polym. J.*, vol. 31, no. 9, pp. 835–839, Sep. 1995.
[63] M. C. Militello and S. J. Simko, "Elemental Palladium by XPS," *Surf. Sci. Spectra*, vol. 3, no. 4, pp. 387–394, Oct. 1994.
[64] E. H. Voogt, A. J. M. Mens, O. L. J. Gijzeman, and J. W. Geus, "XPS analysis of palladium oxide layers and particles," *Surf. Sci.*, vol. 350, no. 1–3, pp. 21–31, Apr. 1996.
[65] G. Ertl, R. Hierl, H. Knözinger, N. Thiele, and H. P. Urbach, "XPS study of copper aluminate catalysts," *Appl. Surf. Sci.*, vol. 5, no. 1, pp. 49–64, May 1980.